# UAV Pilot Status Identification Algorithm Using Image Recognition and Biosignals

Sedam Lee, Eunsung Go, and Yongjin Kwon
Dept. of Industrial Engineering, Ajou University, Suwon, South Korea
Email: {lsd2547, kes0824, yk73}@ajou.ac.kr

***Abstract*—With the development of various technologies such as sensors and communications, the scope of application for UAVs (unmanned aerial vehicles) is expanding. The use of UAVs is increasing not only in the military sectors, but also in the civilian industries. For the operation of UAVs, pilots must use a control system called the GCS (ground control system). With the GCS, pilots need to understand and be informed of the full operational context of the UAVs. However, the GCS can only provide the pilots with limited resources. Therefore, in order to overcome these limitations, excessive information may be provided to the pilots, which may cause abnormal conditions such as mission overload. In this context, there is a need for a system that can prevent abnormal conditions of the pilot and increase the mission success rate. In this paper, the pilot state information is collected through a camera and wearable devices to understand the pilot state in real time. An algorithm that can derive the pilot state from the collected information was developed. Algorithms can provide feedback to prevent accidents caused by mistakes and contingencies that can arise from the pilot's abnormal conditions. The algorithm shows high accuracy and stability when applied to simulated flight conditions. In addition, it is simple to use and there are no physical restrictions on the pilot's action, hence efficient mission performance is expected.**

***Index Terms*—pilot state, abnormal condition, biosignals, face recognition, posture estimation, state identification**

## I. Introduction

Unmanned Aerial Vehicles (UAVs) operate without a pilot on board. Therefore, unlike manned aircraft, where the pilot directly boards and obtains information, it is highly dependent on an operating system called the Ground Control System (GCS). UAVs are basically monitored and controlled through the GCS. Therefore, pilots must always stare at the GCS screen, and control the UAV with attention [1], [2].

The UAV's mission is performed through the screen provided by the GCS in a limited space rather than in the open field [3]. Therefore, as the UAV operation time increases, the pilot may make mistakes due to distraction, fatigue, or carelessness [4]. Due to the characteristics of the UAVs, a simple mistake by the pilot may result in an accident such as personal injury or material damage, which may result in large losses.

Manuscript received April 26, 2022; revised August 10, 2022.

Currently, the GCS used for UAV control only provides notifications and warnings about the UAV's status and flight status. There is no feedback regarding the state of the pilot controlling the UAVs. If the pilot posture can be recognized and the pilot's biosignals can be collected to clearly understand the pilot condition, it is expected that the pilot mistakes can be prevented by providing feedback accordingly [5]-[7]. Therefore, an attempt was made to develop a system algorithm that can identify and derive the current state of the pilot. This is expected to ensure high safety by preventing accidents, and is expected to increase the pilot's mission success rate. In this light, it will be possible to prepare an opportunity to develop a high-safety GCS system by using UAVs in various ways in more diverse industrial activities [8], [9].

The structure of this paper is as follows. Chapter 2 discusses the image recognition technique and biosignal acquisition process. Chapter 3 defines the state variables for estimating the pilot state through the collected information, while Chapter 4 defines the criteria for deriving the pilot state. Chapter 5 describes the algorithm for real-time monitoring of the pilot state. The last chapter describes the experiments and conclusions to verify the designed algorithm.

## II. Collecting Pilot State Information

### A. Pilot's Face Recognition

One of the pieces of information that can be used to recognize a pilot condition is facial expression. This is the data that can be primarily helpful in understanding the pilot condition, such as closing his eyes or yawning. Therefore, the face of the pilot controlling the UAVs is collected through the camera in order to estimate the state through the facial expression. Facial features were used to distinguish the pilot face through the collected images. The position of the eyes, nose and mouth, which are the biggest features of the face, is designated as a Region of Interest (ROI). Then, the pilot facial expression is recognized through the feature points extracted from the ROI.

When image recognition is used, the face must be recognized even in the intervention of various disturbances (varying face directions, ambient light intensities, etc.) that may interfere with the environment. Therefore, it was decided to utilize the unique features of the face to clearly recognize the face in varying conditions. The HOG (histogram of oriented gradients) algorithm was used to define the unique features [10]. A video is a sequence of


doi: 10.12720/jait.13.5.477-485

numerous images according to the number of frames. Therefore, the RGB image for each frame was converted into a GRAY image using the HOG algorithm. In this way, the image brightness changes that can be identified as a change in pixel values through the HOG algorithm is expressed as a gradient. After that, the positioning and projection of the face were carried out. This compensates for the pixel values that change depending on the pilot head directions. In addition, a process for recognizing face images collected by recognizing landmarks such as eyes, nose, and mouth is performed, as in Fig. 1.

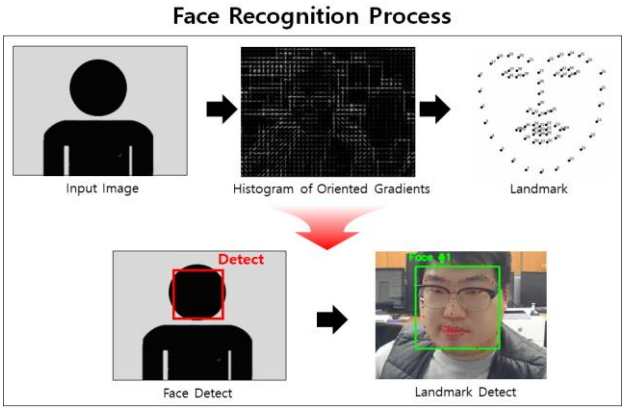


Figure 1. Face recognition process.

For the process, the iBUG 300-W data set, a machine learning model, was applied. A trained facial landmark predictor model was used for face recognition.

### B. Pilot Posture Recognition

In addition to the pilot facial expression, it is possible to grasp the pilot condition through certain actions and postures. However, the pilot posture recognition can be limited due to numerous possible postures, concealment of the body, other object obstruction, and actions that occur outside the camera angle. Therefore, it is more difficult than understanding the state through the pilot face recognition. In this study, the pilot posture was detected using a Machine Learning (ML)-based body recognition method. In order to understand the pilot posture, the landmark, the 2D boundary part of the body of the recognized object, was inferred for each single frame from dozens of frames. After that, the position of the body was defined by matching the skeleton with the landmark. Through this, the MediaPipe's Blaze Pose algorithm was used to estimate the pilot full body posture [11].

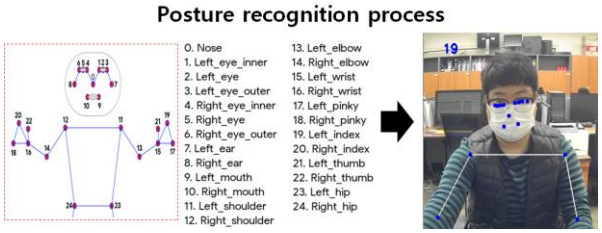


Figure 2. Estimation of the pilot's posture.

The pilot posture estimation algorithm was applied to each single frame, as shown in Fig. 2, to estimate the posture in real time. Even if the pilot's whole body is out of the camera angle, the posture can be estimated by matching the key points of other joints with the skeletal model. Fig. 3 shows the posture estimation pipeline.

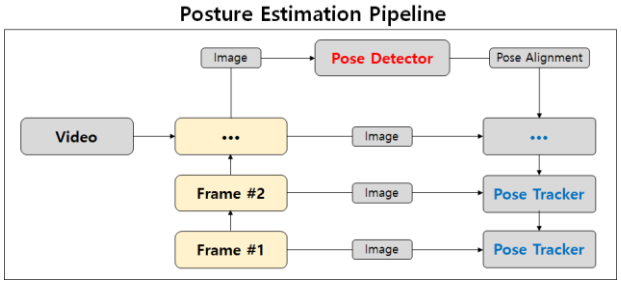


Figure 3. Pilot's posture estimation pipeline.

### C. Pilot's Biosignal Collection

In order to collect the pilot's biometric information, various sensors must be attached to collect the information. However, because the equipment used in the past hinders the pilot movements by attaching a complex and heavy sensors, a wearable device that can be used conveniently is used. Although it has the disadvantage of collecting fewer biosignals compared to the existing devices, it was more suited for the purpose of this study. The wearable device used in this study is the Samsung Galaxy Watch 3 model. It collects the heart rate, which is one of the pilot's biometric information. When the wearable device collects biometric information, it measures the heart rate by using the built-in photo plethysmography (PPG) sensor. Heart rate measurement using a cuff-type blood pressure monitor and wearable device was classified into normal and post-activity states, and heart rate per minute was measured. The average BPM (in Eq. (1)) was obtained by measuring 5 times for each state. The difference between the averages was analyzed and the existing heart rate values were adjusted as correction values applied.

$$BPM_{average} = \frac{1}{n}\sum_{k=1}^{1} BPM = \frac{BPM_1 + \cdots + BPM_n}{n} \quad (1)$$

## III. Variable Measurement to Determine the Pilot State

In this study, to understand the pilot state, it was classified into two types: Normal and Abnormal. Image recognition and biometric information were used to estimate the abnormal state. Therefore, the image information detects the position and condition of the pilot eyes through face recognition, and the biometric information brings the operator's heart rate. In order to estimate the pilot condition through this information, numerical values for each condition are analyzed, and judgment criteria for each abnormal condition are defined.

### A. Eye Aspect Ratio (EAR)

EAR (Eye Aspect Ratio) is one of the main indicators in determining the state of the pilots. In this study, the eye condition of the operator was used as an index to estimate the condition of the pilot. The facial landmark detection-based library is used to recognize the pilot face, find the landmark of the face, and recognize the eye state through

the process of recognizing the position of the eye on the face. Fig. 4 shows the location of landmarks in the eye.

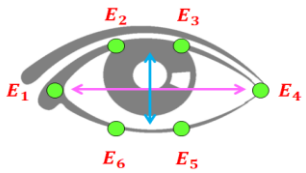


Figure 4. Definition of landmarks in the eye.

$$\text{EAR} = \frac{||E_2 - E_6|| + ||E_3 - E_5||}{2||E_1 - E_4||} \quad (2)$$

EAR, which can determine the state of the eyes through face recognition, was used (as in Eq. (2)). In order to understand the appropriate reference values for this EAR, the numerical values for each state in the image was analyzed through the operation image for each work area on the screen, and the appropriate value was used as the reference index. As shown in Fig. 5, the EAR value was classified through the operation screen for each ROI on the screen, and the average EAR for each state was derived and used by analyzing the EAR for each area.

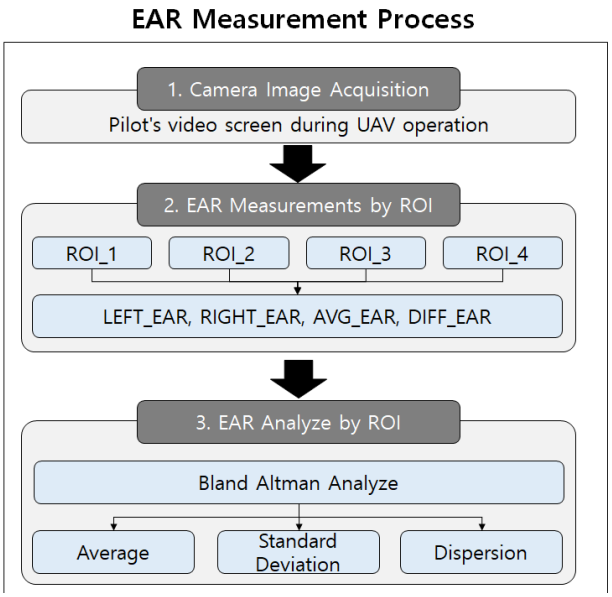


Figure 5. Process for pilot EAR measurements.

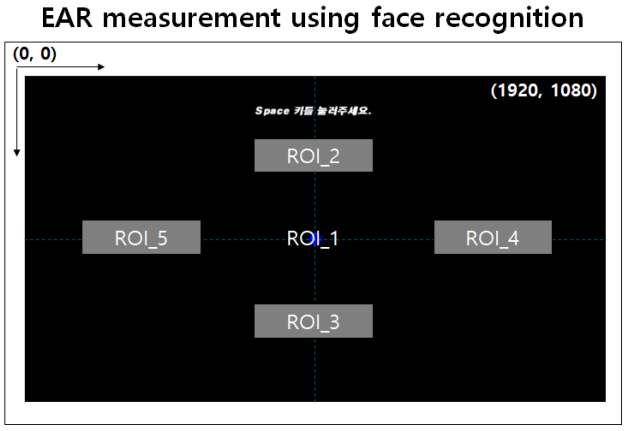


Figure 6. Display for EAR measurement.

Fig. 6 shows the actual measurement screen of the program that can measure EAR by ROI. For each location of the ROI, the pilot looking at the point at that location is collected with a camera. The pilot eye condition is identified through the gaze screen for each ROI.

Through the collected images, the average value of each EAR for the left and right eyes, and the difference between the EARs are derived. The EAR values derived through this process are saved in a CSV file format. After that, the file is delivered to the EAR analysis program. The EAR recognizes the position of the eyes through the landmark of the face recognized on the operation screen. The detected eyes are calculated as in Eq. (2) using the six landmark coordinates, as shown in Fig. 7.

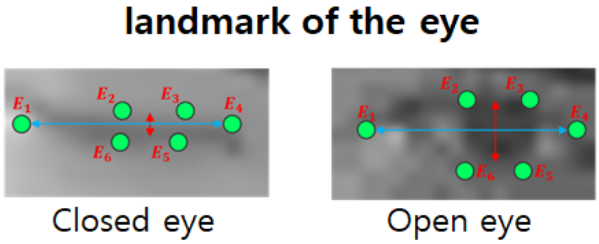


Figure 7. Deriving the pilot's eye state.

Through the EAR, it is possible to determine the values when the pilot eyes are closed and open. Through this, the abnormal state can be derived. In order to define a high-accuracy measurement standard, the average value of the EARs measured by ROI was defined as the state threshold of the final EAR of the unmanned aerial vehicle pilot. This is shown in Table I.

TABLE I. EAR MEASUREMENTS BY ROI

| ROI | Open eyes EAR(Avg) | Closed eyes EAR(Avg) |
|---|---|---|
| 1st. ROI | 0.323323 | 0.206443 |
| 2nd. ROI | 0.316506 | 0.127466 |
| 3rd. ROI | 0.357145 | 0.14307 |
| 4th. ROI | 0.297546 | 0.139888 |
| 5th. ROI | 0.341245 | 0.128734 |
| EAR Avg | 0.327153 | 0.14912 |

As shown in Fig. 8 and Fig. 9, the standard EAR was defined through the measured EAR. The smallest error was measured when the threshold was set as the standard according to the change of the pilot conditions.

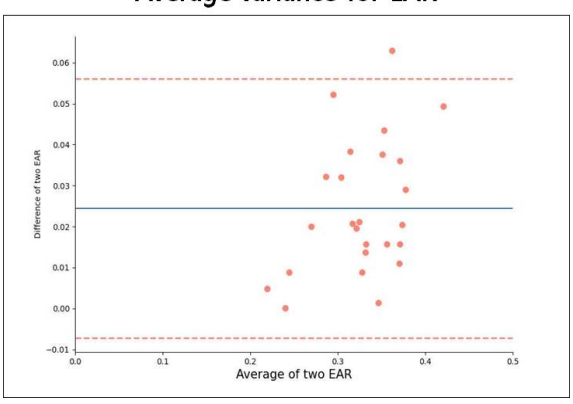


Figure 8. Average variance for EAR.

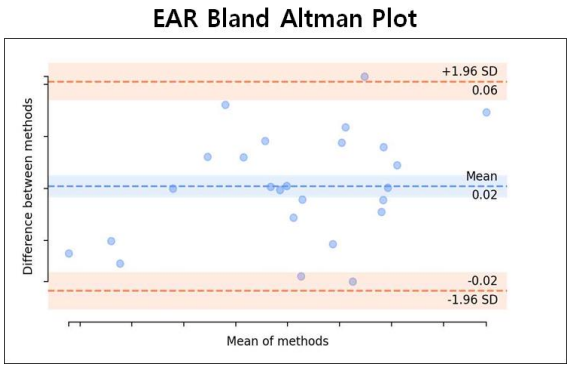


Figure 9. EAR bland & altman plot.

Through the EAR measured according to the pilot conditions, the standard EAR values in the open and closed state were defined and used as one of the indicators to judge the normal and the Abnormal state. Table II illustrates the variable values in accordance with the eye conditions.

TABLE II. VARIABLE VALUES ACCORDING TO EYE CONDITIONS

| List | Open eyes | Closed eyes |
|---|---|---|
| Mean | 0.024454 | 0.013589 |
| Standard Deviation | 0.016106 | 0.013191 |
| Variance | 0.000259 | 0.000174 |

In order to determine whether there is a drowsiness, which is one of the abnormal behavior states, a judgment is made through the formula (Eq. (3)) together with the EAR indicator.

$$Drowsiness\ State = \frac{N_{Alert}}{1FPS} \tag{3}$$

$N_{Alert}$ represents the number of durations of the behavioral alert state for 1 fps, which means when the EAR value drops below the standard for closed eyes. In the collected camera image, if the duration of this state exceeds 70% based on fps, it is the warning stage. If it exceeds 90%, it is designated as an alert stage and divided into detailed states according to the severity of the abnormal behavior state, as in Table III.

TABLE III. STEP-BY-STEP DROWSINESS STATE

| State | Ratio (%) |
|---|---|
| Warning | 70(%) |
| Alert | 90(%) |

### B. Body-Face Ratio (BFR)

Body-Face Ratio (BFR) is a value to define the attitude variable for the pilot state part collected on the camera screen during GCS operation of the unmanned aerial vehicle. When the posture of the pilot controlling the unmanned aerial vehicle changes, the shoulder spacing of the upper body shows a constant value. It also means the ratio of these two figures based on the change in the distance difference from the face. In this study, the position of each joint was identified through the operator posture recognition, and the amount of change in BFR was analyzed and used as one of the indicators to define the pilot's current posture. The key point location and definition are given in Fig. 10.

$$\text{BFR} = \frac{||B_0 - B_1||}{||B_2 - B_3||} \tag{4}$$

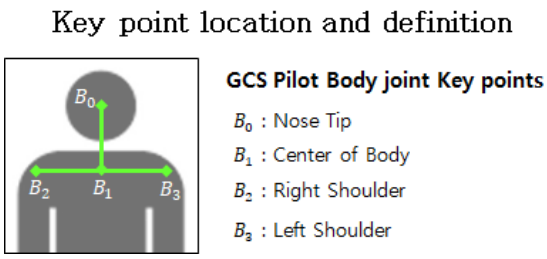


Figure 10. Key points and definitions.

In this study, BFR was used as an index to determine the pilot's current posture using the joint position of the posture (Eq. (4)). This can be seen in Fig. 11. The BFR value changes according to the change of the pilot posture, which is to measure the aspect ratio through the position of the body and face by collecting the position information of each joint using the Pose API provided by MediaPipe [11].

B1 is the center point of both shoulder joints, and BFR is defined as the aspect ratio based on B2-B3 and B0-B1. Fig. 12 and Fig. 13 show the change of the shoulder according to the direction, in which the pilot looks at the screen.

The ROI area on the screen was divided into three parts (i.e., left, center, and right), and the operation screen was continuously captured, while the pilot was looking at the area. The average coordinate distance values between B2-B3 for each ROI were compared for a certain period of time.

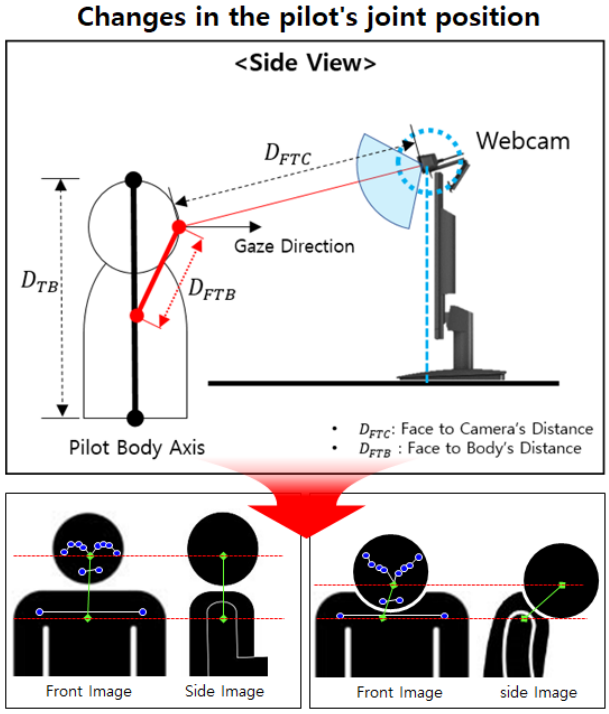


Figure 11. Key points according to posture changes.

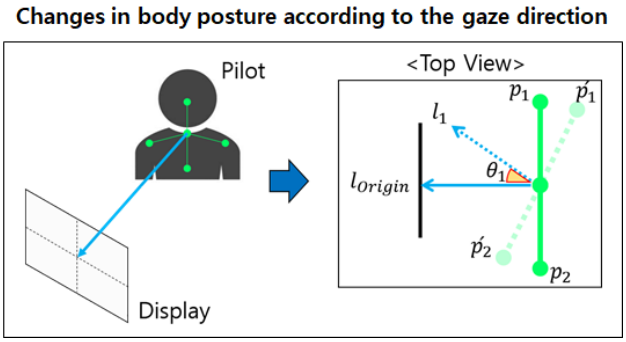


Figure 12. Shoulder change according to gaze direction.

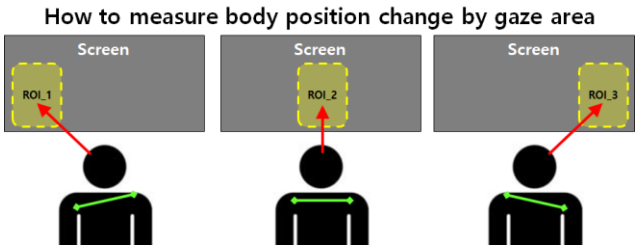


Figure 13. Change of body position according to ROI area gaze.

Based on the FHD resolution for each ROI area, it was confirmed that the difference in image coordinates for the B2-B3 interval was about 5 pixels. The shoulder width of the subject measured as a frontal standard is about 44 cm, and a five-pixel difference on the image coordinates indicates a change within 1 cm based on the measured result value. Therefore, the change in the longitudinal length of the body according to the position to be observed according to the work is negligible. This is shown in Fig. 14.

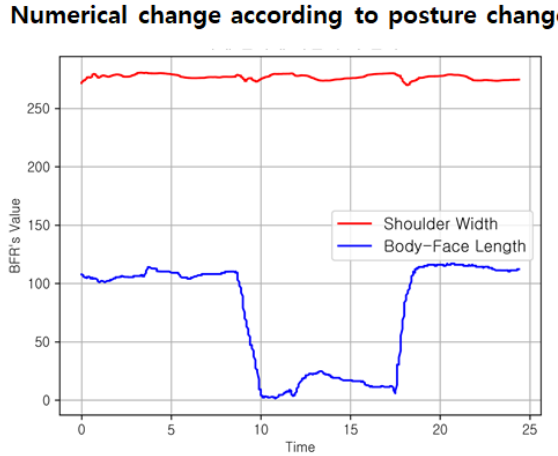


Figure 14. Numerical change according to posture change.

TABLE IV. BFR VALUES BY STATE

| Number | Normal (BFR) | Drowsiness (BFR) |
|---|---|---|
| 1 | 0.455138 | 0.128096 |
| 2 | 0.454272 | 0.155723 |
| 3 | 0.463585 | 0.074218 |
| 4 | 0.471524 | 0.061614 |
| 5 | 0.454478 | 0.114493 |
| Total Avg | 0.459799 | 0.106829 |

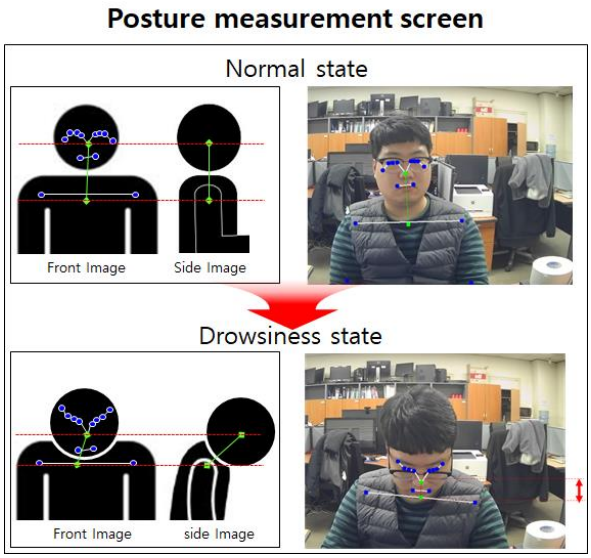


Figure 15. BFR measurement screen according to state.

It was confirmed that the change in 'Shoulder Width' was insignificant, when changing from the normal posture to the prone position, while the change in 'Body-Face Length' was large. Through these numerical changes, the posture can be estimated by grasping the aspect ratio values according to the changes in the operator posture. By dividing the pilot posture into the normal state and the prone state, the BFR is obtained and the aspect ratio for each posture is defined, as shown in Fig. 15. The BFR values for each posture were derived by measuring the average BFR value per hour by measuring a total of 5 times for 1 minute for each posture. As a result of the measurement in the normal state, values between 0.45 and 47 were distributed and detected, as in Table IV. Through this, it was confirmed that the BFR standard was maintained above 0.45 in the normal state. Therefore, the reference index value of the BFR general state was defined as 0.45. As a result of the measurement in the prone position, it is distributed between 0.06 and 0.15. It can be seen that the number differs depending on the degree to which the head is bowed. The reference index value in the prone state was defined as 0.15 using the distribution average of the highest value.

### *C. Heart Rate (BPM)*

BPM, which represents the heart rate per minute, represents a heart rate of 60-100 beats per minute in a normal state (resting period) based on a healthy adult standard. Since this heart rate changes rapidly due to physiological phenomena such as exercise, anxiety, tension, and stress, the changes in heart rate per minute can be used as an index for mental and physical abnormalities. In this study, the operator's biosignal information was collected through a commercial wearable device, and BPM (as in Eq. (5)) was extracted and used as one of the indicators to determine the operator's abnormal condition.

$$BPM(Beats\ per\ Minute) = \frac{60}{R-R}(bpm) \quad (5)$$

When the average heart rate per minute for each state is measured, it shows a certain difference between the

wearable device and the cuff type blood pressure monitor. This difference was applied as a correction value of the sensor value of the wearable device, and the heart rate of the final pilot was extracted and applied. Table V shows the BPM in accordance with the state.

TABLE V. BPM ACCORDING TO STATE

| | Normal | | Activity | |
|---|---|---|---|---|
| | cuff | wearables | cuff | wearables |
| 1st. | 82 | 85 | 102 | 105 |
| 2nd. | 81 | 84 | 100 | 104 |
| 3rd. | 80 | 83 | 101 | 104 |
| 4th. | 83 | 86 | 103 | 105 |
| 5th. | 82 | 85 | 102 | 106 |
| Avg. | 81.3 | 84.6 | 101.6 | 104.8 |

## IV. DEFINING CRITERIA FOR STATE IDENTIFICATION

In controlling an unmanned aerial vehicle, the pilot state can be largely divided into a normal state and an abnormal state. If a pilot can control the unmanned aerial vehicle normally without any problem, it is defined as a normal state. In addition, a case in which a problem occurs in controlling the unmanned aerial vehicle is defined as an abnormal state. The steady state and the abnormal state are classified as shown in Table VI, and standard indicators for each should be presented.

TABLE VI. PILOT STATE CLASSIFICATION

| Behavior State | | | | | | |
|---|---|---|---|---|---|---|
| Normal | | Abnormal | | | | |
| Idle | Prone | Idle | Prone | AWOL | Risk | Error |
| Normal Working Condition | | Sleep | | Out of C ockpit | Heart D anger | Not w orn |
| | | Distracted Operation | | | | |

Fig. 16 shows the measured variable values according to each state.

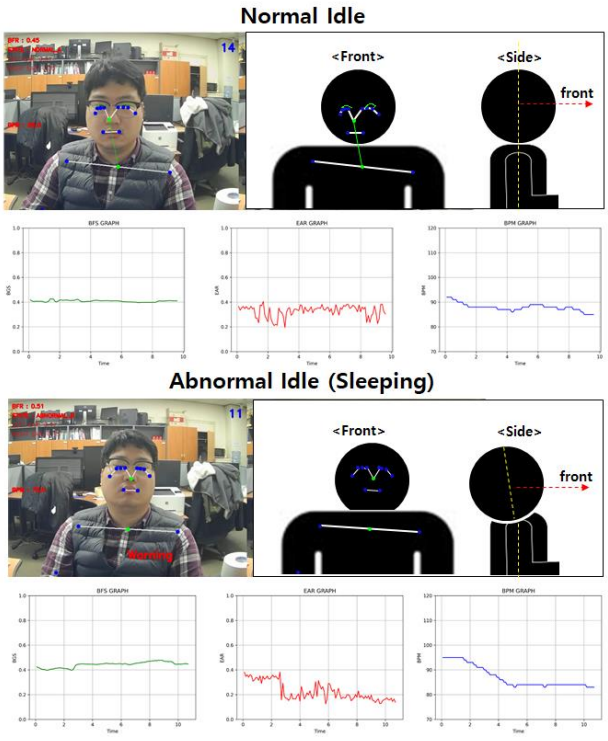


Figure 16. State measurement screen.

When the pilot is in a normal state, it could be confirmed that BFS kept constant over 0.4. Although the EAR fluctuates, it is generally maintained above 0.35, and the BPM also maintains a constant value. In the abnormal state (e.g., sleep state), unlike the previous normal state, it can be seen that the EAR drops from 0.35 to 0.2 or less. You can see the graph where the BPM also gradually decreases. Therefore, the state of the unmanned aerial vehicle pilot is defined as shown in Table VII, Table VIII and Table IX on the criteria for defining the state through the previously measured variable values.

TABLE VII. DEFINING CRITERIA BY PILOT STATE_1

| Behavior State | Pilot Behavior | EAR |
|---|---|---|
| Normal | Idle | $0.32 < S_{EAR}$ |
| | Prone | Not Detected |
| Abnormal | Idle | $0.14 < S_{EAR}$ |
| | | Not Detected |
| | Prone | Not Detected |
| | | Not Detected |
| | AWOL | Not Detected |
| | Danger | Don't Care |
| | Equipment Error | Don't Care |

TABLE VIII. DEFINING CRITERIA BY PILOT STATE_2

| Behavior State | Pilot Behavior | BFR |
|---|---|---|
| Normal | Idle | $0.15 < S_{BFR} < 0.45$ |
| | Prone | $S_{BFR} < 0.15$ |
| Abnormal | Idle | $0.45 < S_{BFR}$ |
| | | $0.45 < S_{BFR}$ |
| | Prone | $S_{BFR} < 0.15$ |
| | | $S_{BFR} < 0.15$ |
| | AWOL | Not Detected |
| | Danger | Don't Care |
| | Equipment Error | Don't Care |

TABLE IX. DEFINING CRITERIA BY PILOT STATE_3

| Behavior State | Pilot Behavior | BPM |
|---|---|---|
| Normal | Idle | $60 < S_{BPM} < 100$ |
| | Prone | $60 < S_{BPM} < 100$ |
| Abnormal | Idle | $60 < S_{BPM} < 80$ |
| | | $60 < S_{BPM} < 100$ |
| | Prone | $60 < S_{BPM} < 80$ |
| | | $60 < S_{BPM} < 70$ |
| | AWOL | Not Detected |
| | Danger | $60 > S_{BPM}$ or $S_{BPM} > 110$ |
| | Equipment Error | Not Detected |

## V. PILOT STATE DETERMINATION ALGORITHM

In order to detect the state of the unmanned aerial vehicle pilot, video information is collected using a camera, and bio-signals are collected using a wearable device. To determine the pilot state while the pilot is controlling the unmanned aerial vehicle, it is necessary to collect information in real time, analyze the information, and finally derive the state. In this study, three major indicators were used to determine the pilot condition. The pilot expression through image recognition was used as the first index, and the second index is the pilot behavior. The third and final indicator used the heart rate, which is a vital signal. For each of the three indicators, the cloud server of AWS (Amazon Web Service) was used for the collection and pre-processing to proceed simultaneously through

each collection process. After implementing the DB through the cloud server, the conditional statements for deriving each state were implemented in Python. Since the pilot state identification algorithm derives the state through three pieces of information, EAR, BFR, and BPM were visualized to understand the pre-processing process at the same time as the information collection. This is shown in Fig. 17.

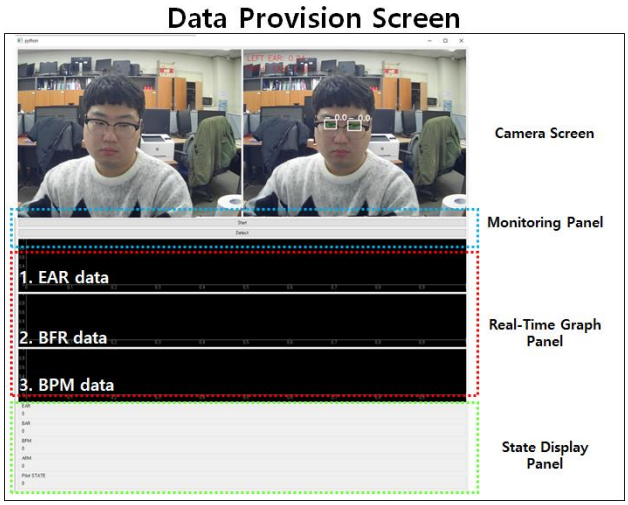


Figure 17. Real-time pilot state screen.

Fig. 18 shows the schematic diagram of the unmanned aerial vehicle pilot state detection algorithm.

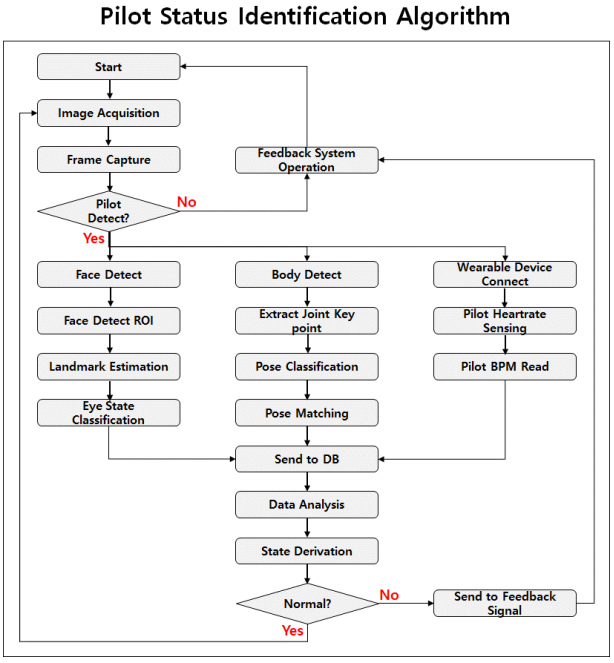


Figure 18. Schematic diagram of real-time pilot state identification algorithm.

## VI. Algorithm Verification through Experimentation

To verify the pilot state identification algorithm, the accuracy of the UAV GCS simulation algorithm and the judgment results through the algorithm were analyzed. As shown in Table X, the 'actual' means the actual value (pilot behavior), and the 'predicted' means the determined behavioral state. TP (true positive) is when an abnormal behavior is correctly detected, TN (true negative) is when a normal behavior is not detected as an abnormal behavior. FP (false positive) is when a normal behavior is detected as an abnormal behavior. FN (false negative) means that the abnormal behavior is not detected as an abnormal behavior.

TABLE X. Prediction Error Table

| Actual \ Predicted | Positive | Negative |
|---|---|---|
| Positive | True Positive | Fallse Negative |
| Negative | False Positive | True Negative |

$$\text{Sensitivity} = \frac{TP}{TP + FN} \tag{6}$$

$$\text{Specificity} = \frac{TN}{TN + FP} \tag{7}$$

In the GCS simulation experiment result, the sensitivity indicates the number of detections for abnormal behavior (in Eq. (6)). It means that the higher the number, the higher the probability of detection of abnormal behavior. Specificity indicates the number of times that normal behavior and abnormal behavior were judged (in Eq. (7)). It means that the higher the number, the better the distinction between normal behavior and abnormal behavior. In this paper, the accuracy of the monitoring system is evaluated using the sensitivity and specificity, as in Table XI. Operational images were collected for each action within the range that can be simulated, and the evaluation was conducted based on the results of determining the action for successive frames.

TABLE XI. Measured Sensitivity, Specificity

| State | Behavior | Sensitivity | Specificity |
|---|---|---|---|
| Normal | Idle | 99.49 | 99.49 |
| | Prone | 99.49 | 98.98 |
| Abnormal | Idle (Drowsiness) | 92.66 | 91.84 |
| | Idle (Distracted Operation) | 93.66 | 95.41 |
| | Prone (Drowsiness) | 95.42 | 96.77 |
| | Prone (Sleep) | 94.07 | 98.98 |
| | AWOL | 97.46 | 95.41 |
| | Equipment Error | 98.98 | 98.95 |

In the operation of the UAVs, it was confirmed that high sensitivity and specificity were obtained in the behavioral judgment in the normal state, respectively. It can be seen that, in determining the behavioral state in the normal state, the pilot who takes the upright posture has a higher recognition rate of face and posture, resulting in such a result. It was confirmed that the accuracy of the behavioral state judgment in the abnormal state is slightly lower than that in the normal state. It can be seen that the specificity in the prone state, where the recognition of abnormal behavior judgment is relatively simple, is higher than the classification in the idle state. It was confirmed that, in the judgment in which the eye state information is additionally

added along with the posture information, the smaller the judgment variable in the classification, the higher the accuracy. It is also possible to check that both Sensitivity and Specificity are high in a state that can be judged by one state variable, such as an equipment error. Through these results, it was confirmed that the less state variables or the more clearly recognizable state, the higher the accuracy in judging the operator's abnormal behavior.

## VII. Results and Conclusions

In order to build a system that derives the pilot state in real time, we developed an image information collection system and a biometric information collection system to collect necessary data. Based on these data, we derived a reference index for judging abnormal behavior through measurement. In addition, these indicators were applied to each algorithm for judging abnormal behavior. This allows the operator to determine normal and abnormal behaviors. Using the system proposed in this paper, the environment can be configured more simply than the existing monitoring system configuration through webcams and wearable devices. However, it was difficult to obtain more diverse data in limited experimental subjects and experimental settings. By improving these parts, it will be possible to identify states with higher accuracy, and more diverse states can be derived.

In the future, if any research is conducted to more accurately derive the pilot conditions in real time through eyes, body posture, and biosignals, a guideline for providing a warning sound to alert a pilot in a drowsy state. If additional research is conducted on a feedback system that provides customized feedback according to the pilot conditions, the pilot state derivation algorithm can show more meaningful results by increasing the safety of UAV operation and minimizing risks. In particular, if the pilot state is derived more diversely and research is conducted to provide appropriate feedback for each derived state, it can be of great help in increasing the mission success rate.

## Conflict of Interest

The authors declare no conflict of interest.

## Author Contributions

The first author, Sedam Lee, has conducted the research, including the generation of research idea, formulate the research process, and written the major portion of the manuscript; the second author, Eunsung Go, has come up with the experimentation plans, fine-tuned the plans, and actually conducted the experimentations, while composed the computer code to analyze the data; the third author, Yongjin Kwon, has validated the analysis results, corrected the manuscript in terms of overall structures and English grammars. Also, all authors have approved the final version.

## Acknowledgment

This research was supported by Unmanned Vehicles Core Technology Research and Development Program through the National Research Foundation of Korea (NRF) and Unmanned Vehicle Advanced Research Center (UVARC) funded by the Ministry of Science and ICT, the Republic of Korea (Grant Number: 2020M3C1C1A01084900).

## References

[1] ACC, "ASAP," *Air Combat Command's Safety Magazine Combat Edge (Spring Edition)*, p. 14, 2017.
[2] S. Bordenave, "The proper use of Military Flight Operations Quality Assurance (MFOQA) analysis and unstable approach rates," *AMC*, 2014.
[3] S. Qi, F. Wang, and L. Jing, "Unmanned aircraft system pilot/operator qualification requirements and training study," *MATEC Web of Conferences*, vol. 179, 2018.
[4] H. Huang, "Autonomy Levels for Unmanned Systems (ALFUS) framework: Safety and application issues," in *Proc. the Workshop on Performance Metrics for Intelligent Systems*, 2007, pp. 48-53.
[5] J. Feng, Z. Guo, J. Wang, and G. Dan, "Using eye aspect ratio to enhance fast and objective assessment of facial paralysis," *Computational and Mathematical Methods in Medicine*, vol. 2020, 2020.
[6] K. Khabarlak and L. Koriashkina, "Fast facial landmark detection and applications: A survey," arXiv preprint arXiv:2101.10808, 2021.
[7] V. Bazarevsky, *et al.*, "BlazePose: On-device real-time body pose tracking," ARXIV: arXiv:2101.10808, 2021.
[8] L. Jimenez, A. Parnandi, and R. Gutierrez-Osuna, "Extracting heart rate and respiration rate using a cell phone camera," *Computer Science*, 2013.
[9] K. Swieringa, R. Young, and G. Hunter, "UAS concept of operations and vehicle technologies demonstration," in *Proc. Integrated Communications, Navigation and Surveillance Conference*, 2019, pp. 490-504.
[10] T. Blumer, C. Wargo, and G. Hunter, "UAS situation awareness shortcomings, gaps, and future research needs," in *Proc. Integrated Communications, Navigation, Surveillance Conference*, 2018, pp. 2G1-1-2G1-8.
[11] W. Zhang, J. Shirley, Y. Deng, N. Kim, and D. Kaber, "Effects of dynamic automation on situation awareness and workload in UAV control decision tasks," in *Proc. International Conference on Applied Human Factors and Ergonomics*, 2018, pp. 193-203.



**Sedam Lee** has many years of engineering experience in industrial engineering. He has conducted research applied to industrial engineering concepts in military and simulation. He has a major interest in the fields of simulation, unmanned systems, and UAV. He has studied his master's degree at Ajou University.

**Eunsung Go** has various experiences in image recognition in the field of industrial engineering. He has conducted various researches applying image recognition technology to unmanned aerial vehicles, ground control systems, and simulations. He has great interests in the fields of simulation, unmanned systems and UAVs. He obtained his master's degree from Ajou University.

**Yongjin Kwon** has many years of engineering experience in industrial and academic settings. He has extensive experience & practical knowledge in current design, manufacturing and quality control. His work has been cited a number of times in high profile journals. He is currently a professor in the Department of Industrial Engineering at Ajou University. Prior to joining Ajou, he was on the faculty of Drexel University.